

A Novel Modeling Technique for Efficiently Computing 3-D Capacitances of VLSI Multilevel Interconnections—BFEM

Hsin-Ming Hou, *Student Member, IEEE*, Chin-Shown Sheen, *Student Member, IEEE*,
and Ching-Yuan Wu, *Member, IEEE*

Abstract— An efficient method is presented to model the parasitic three-dimensional (3-D) capacitance of VLSI multilevel interconnections. Based on the boundary-finite-element method (BFEM) of integral formulation, arbitrary triangle elements on the surface of conductors for charge distribution are used to efficiently calculate capacitances of both parallel conductors and complicated configurations such as crossing lines, corners, contacts, and their combinations. Using an adaptive multilevel Green's function and low-order polynomials as shape function, we apply the Galerkin principle over finite elements, and most of the surface integrals of charge distribution can be evaluated analytically and the singular integrals can be eliminated by choosing proper coordinate transformation. Moreover, an even less complex and more general method for arbitrary geometry configuration of multilevel interconnection lines is proposed in order to link with the finite element pre-processor in present CAD tools.

Index Terms— BFEM, Green's function, interconnection, 3-D capacitance, VLSI.

I. INTRODUCTION

AS THE feature sizes of devices are scaled down, the response time of VLSI chip is increasingly dominated by the interconnection [1], [2]. The computation of capacitances between different metal layers for such a densely packed multiconductor system is a complex and difficult task. Several methods [3]–[20] have been developed in the past, and for FD [3]–[6] and FE [7] methods, the charge density diverges at the sharp edges and the solution of Poisson's equation requires an artificial bounded region that is difficult to determine. Most of them treat the two-dimensional (2-D) problems, in which infinite parallel conductors are considered [3], [4], [14]. For three-dimensional (3-D) problems, the method most commonly used is to solve the Green's function integral equation by "point fitting method" [15] or the "finite element technique" [7]–[10], [16]. The charge distribution proposed in [11]–[13] consists of constant surface charges on the rectangular grid of conductor boundaries. The problems with this method are that a large set of functions is needed to approximate the charge distribution and high-order integrals have to be

evaluated. Recently, an efficient modeling based on piecewise-linear charge distribution concentrated on a network of edges was presented in [8]–[10]. Using this technique, the order of integration is reduced to one but singularity problem of the concentrated charges on edges can't be eliminated and may lead to erroneous results [10]. On the other hand, fast empirical models have also been proposed [22], but they are not accurate enough, particularly for estimating 2-D and 3-D capacitance coefficients.

Based on the boundary-finite-element method (BFEM) of integral formulation [10], we use arbitrary triangle elements on the surface of conductors for charge distribution. Hence it is easy to calculate capacitances of both parallel conductors and complicated configuration such as crossing lines, corners, contacts, and their combinations. Using an adaptive multilayer Green's function and low-order polynomials as shape function, we apply the Galerkin principle over finite elements. Most of the surface integrals of charge distribution can be evaluated analytically, therefore the singularity problems can be eliminated and analytical solution can be obtained.

A 3-D capacitance modeling for an arbitrary structure has been developed and is confirmed to be efficient and accurate as compared with existing data. Major improvements for this purpose are adoption of arbitrary triangle elements and elimination of singular integrals to obtain analytical form. These improvements have made it possible to link with CAD tools.

Our paper is organized as follows. Section II is devoted to mathematical formulation of capacitance suitable for 3-D multiconductor system. Using Fourier integral technique, Green's function and the discretization of potential formulation are described. Furthermore, reduced capacitance matrices are presented. The manipulation of the integration for different cases including singular integration, neighboring singular integration and regular integration are analyzed. Comparisons with other approaches are made in Section III. Conclusions are summarized in the final section.

II. MATHEMATICAL FORMULATION

Consider a configuration of M multilevel interconnection above a ground plane and its equivalent circuit shown in Fig. 1. For this configuration, a $M \times M$ capacitance matrix, C_{ij} , is used to describe the capacitance of nodal admittance matrix. Therefore, C_{ij} will not be extracted directly, one

Manuscript received April 25, 1997; revised June 23, 1997. The review of this paper was arranged by Editor M. Fukuma. This work was supported by the National Science Council under Contract NSC86-2215-E009-034.

The authors are with the Advanced Semiconductor Device Research Laboratory and Institute of Electronics, National Chiao-Tung University, Hsinchu 300, Taiwan, R.O.C.

Publisher Item Identifier S 0018-9383(98)00278-0.

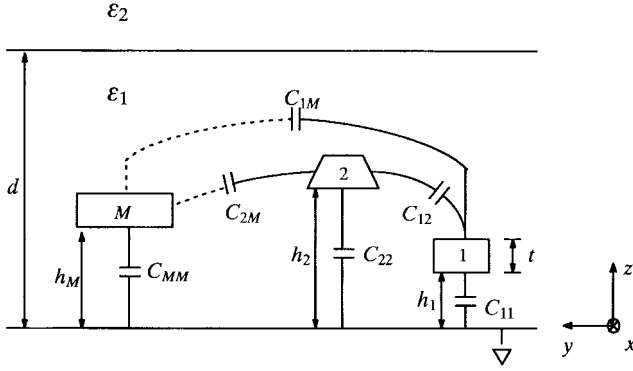


Fig. 1. The configuration of M multilevel interconnections above a ground plane and its equivalent circuit.

has to derive the short-circuit capacitance matrix $C_{s_{ij}}$, as defined and well-known in textbooks. There is a simple relationship between the capacitance matrix and the short-circuit capacitance matrix, and they can be transformed into each other by an incidence matrix [8].

To calculate the capacitance coefficients, the electrostatic potentials for conductors have to be analyzed, which is induced by the charges distributed over the whole space. For the present case, we consider only the surface charge σ on the conductors, therefore the potentials can be formulated in surface integral equations by Green's theorem [11]–[13]. For different configurations of interest in integrated circuits, we have to only choose the appropriate Green's function for the integral equation.

A. Discretization of Potential Formulation

Reducing the Green's integral equation to a discrete problem, we obtain an approximated solution of potential from the discretization of charge on the surface of conductors. Based on the BFEM of integral formulation [10], we use arbitrary triangle elements on the surface of conductors for charge distribution. The integration of charge distribution over all the surface of conductors is then divided into several triangle element integrations to achieve high efficiency. The representation points and nodes are selected on the surface of each conductor. With each node, charges distribute over the triangle elements defined by the arbitrary two near neighboring nodes, the electrostatic potential at the field point $p_{j,jl}$ can be rewritten in a discretization form

$$V(p_{j,jl}) \cong \sum_{i,\tilde{l},\tau} \int_{s_{i,\tilde{l},\tau}} G(p_{j,jl}, q_{i,\tilde{l},\tau}) \sigma(q_{i,\tilde{l},\tau}) ds_{i,\tilde{l},\tau} \quad (1)$$

where $q_{i,\tilde{l},\tau}$ is the space variable used to describe the source point distribution on the τ th nearest-neighboring element of the i th node on the i th conductor.

For brief editing, we let $q_{i,\tilde{l},\tau}$ be replaced by q . Each element of nodes is associated with a shape function, as shown in Fig. 2, to describe the charge distribution of arbitrary triangle elements on the surface of conductors. To simplify the integral equation for the i th node, the shape function at the τ th element of arbitrary triangle is given in a slope-intercept

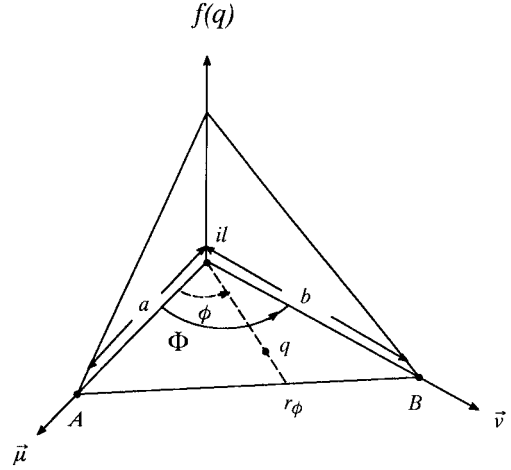


Fig. 2. An evaluation of the shape function amplitude $f(p)$ for the τ th element, the i th node on the surface of the i th conductor.

form by (see Fig. 2)

$$f_{i,\tilde{l},\tau}(q) = A_{i,\tilde{l}} \left[1 - \frac{r(q)}{r_\phi(q)} \right] \quad (2)$$

where

$$r_\phi = \frac{ab \sin \Phi}{a \sin \phi + b \sin(\Phi - \phi)}. \quad (3)$$

Note that $a = a(q)$, $b = b(q)$, and $\Phi = \Phi(q)$; r is the distance between the i th node and the source point q . ϕ and Φ are the angles in the τ th element of arbitrary triangle, as shown in Fig. 2. While a and b are the edge lengths of triangle, which are from the i th node to the other two neighboring nodes. $A_{i,\tilde{l}}$ is a normalization factor and the normalization condition is

$$\sum_{\tau} \int_{s_{i,\tilde{l},\tau}} f_{i,\tilde{l},\tau}(q) ds_{i,\tilde{l},\tau} = 1. \quad (4)$$

Substituting (2) into (4), it gives

$$A_{i,\tilde{l}} = \frac{1}{\sum_{\tau} \frac{a_\tau b_\tau \sin \Phi_\tau}{6}}. \quad (5)$$

As a consequence, the charge distribution on the i th node of the i th conductor will be described by a linear combination of shape functions for the τ th element with the appropriate weights of first-order polynomials. The charge distribution $\sigma_{i,\tilde{l}}(q)$ over the elements can be written as

$$\sigma_{i,\tilde{l}}(q) = \alpha_{i,\tilde{l}} \sum_{\tau} f_{i,\tilde{l},\tau}(q) \quad (6)$$

where $f_{i,\tilde{l},\tau}$ is the shape function of the τ th element, the i th node on the i th conductor; $\alpha_{i,\tilde{l}}$ are the unknown coefficients.

B. Multilayer Green's Function

We assume that the interconnections are placed in a stratified medium. This assumption is valid when the substrate is heavily doped and the IC is reasonably planar. So, the Si-substrate is the infinite ground plane and the SiO_2 layer is used as protective material. We use the Fourier integral technique

[8]–[10] to obtain the Green's function for Si-SiO₂ system shown in Fig. 1. When both the field point and the source points are in the same protective coating such as oxide, the Green's function can be written as

$$G(p, q) = \frac{1}{4\pi\epsilon_1} \left\{ \frac{1}{\sqrt{(x-x')^2 + (y-y')^2 + (z-z')^2}} - \frac{1}{\sqrt{(x-x')^2 + (y-y')^2 + (z+z')^2}} + \sum_{n=0}^{\infty} (-1)^n \left(\frac{\epsilon_1 - \epsilon_2}{\epsilon_1 + \epsilon_2} \right)^{(n+1)} \cdot \left[\frac{1}{\sqrt{(x-x')^2 + (y-y')^2 + [2(n+1)d - (z+z')]^2}} - \frac{1}{\sqrt{(x-x')^2 + (y-y')^2 + [2(n+1)d + (z+z')]^2}} + \frac{1}{\sqrt{(x-x')^2 + (y-y')^2 + [2(n+1)d + (z+z')]^2}} - \frac{1}{\sqrt{(x-x')^2 + (y-y')^2 + [2(n+1)d - (z+z')]^2}} \right] \right\} \quad (7)$$

where ϵ_1 denotes the permittivity of SiO₂; ϵ_2 denotes the permittivity of vacuum; and d is the thickness of SiO₂. The source point $q(x', y', z')$ and the field point $p(x, y, z)$ are space variables, which are described in the rectangular coordinate, as shown in Fig. 1. In (7), the physical meaning of potential can be divided into three terms: the first term is the contribution from the uniform dielectric ϵ_1 ; the second term can be considered as the contribution from the infinite ground plane; while the third term represents the contribution from different dielectrics.

C. Derivation of Capacitance Matrix

If the Green's function (7) and the charge density (6) are substituted into (1), then the potential $V(p_{j,jl})$ at the j th node of the j th conductor is read as

$$V(p_{j,jl}) = \sum_{i=1}^M \sum_{il=1}^{N_i} \alpha_{i,il} P_{i,il,j,jl} \quad (8)$$

where

$$P_{i,il,j,jl} = A_{i,il} \sum_{\tau} \int_{s_{i,il}} G(p_{j,jl}, q_{i,il}, \tau) \cdot \left[1 - \frac{r(q)}{r_{\phi}(q)} \right] ds_{i,il}(q). \quad (9)$$

The standard form for the short-circuit capacitance matrix $[C_S]$ is obtained as [8], [9]

$$[C_S] = [F]^T [P]^{-1} [F] \quad (10)$$

where $[F]$ is introduced as a $\Gamma \times M$ incidence matrix of nodes and conductors; N_i is the total number of nodes. The matrix element F_{ji} is equal to 1 if the i th conductor contains the j th

node, and else $F_{ji} = 0$. $[P]$ is the $\Gamma \times \Gamma$ matrix of the surface integrals.

It should be noted that the inverse matrix $[P]^{-1}$ only depends on geometric configuration of interconnection. It is realized reasonably that the short-circuit capacitance matrix $[C_S]$ is obtained without solving charge distributions and bias voltages. Furthermore, the capacitance matrix $[C]$ can be obtained from $[C_S]$ by an incidence matrix [8].

D. Element Integrations

The integral of matrix element $P_{i,il,j,jl}$ in (9) is the most critical part of simulator, since it determines the computing time and accuracy. We use the same manipulation for the source point and its image point in (9). Hence, we derive the general integral form for one of infinite terms in (9), which can be characterized into three classes. Each one of the three classes is just one of the infinite summation terms. For the surface integral terms denoted as $I = \int (1/r(p, q)) \cdot [1 - (r(q)/r_{\phi}(q))] ds_{i,il}(q)$, we can classify these integrations into three classes of integral formulation.

Class 1 – Singular Integration: The source point q coincides with the field point p . Using polar local coordinate, the local original point is set to the source point q , and the surface integral I has an analytical solution

$$I = \frac{ab \sin \Phi}{2c} \ln \left| \frac{b \sin \Phi + (a - b \cos \Phi + c) \tan \frac{\Phi}{2}}{b \sin \Phi + (a - b \cos \Phi - c) \tan \frac{\Phi}{2}} \right| \quad (11)$$

where $c^2 \equiv a^2 + b^2 - 2ab \cos \Phi$.

Class 2 – Neighboring Singular Integration: One of the neighboring of the source point q coincides with the field point p . Under polar local coordinate, while we have to choose the field point as the local original point in order to reduce to one-dimensional (1-D) integral and I is expressed as

$$I = \int_0^{\Phi} \frac{r_{\phi} \sqrt{c^2 + r_{\phi}^2 - 2cr_{\phi} \cos \phi}}{2b} d\phi \quad (12)$$

where b and c are the geometrical constants of triangular element, which are the same definitions as Class 1 and the variables of ϕ , Φ and r_{ϕ} have to be calculated according to the redefined local coordinate.

Class 3 – Regular Integration: The integration contains no singularities. For an arbitrary triangular element, the 2-D integral is easily reduced to one by integration along the contour of equal amplitude of shape function. I is expressed as

$$I = \frac{b \sin \Phi}{c} \cdot \int_0^a \left(1 - \frac{\mu}{a} \right) \ln \left| \frac{\sqrt{b_1 \mu^2 + b_2 \mu + b_3} + b_4 \mu + b_5}{\sqrt{a_1 \mu^2 + a_2 \mu + a_3} + a_4 \mu + a_5} \right| d\mu \quad (13)$$

where $a_1 = 1$, $a_2 = 2(\Delta x \cdot \mu_1 + \Delta y \cdot \mu_2 + \Delta z \cdot \mu_3)$, $a_3 = \Delta x^2 + \Delta y^2 + \Delta z^2$, $a_4 = \mu_1 \cdot m_1 + \mu_2 \cdot m_2 + \mu_3 \cdot m_3$, $a_5 = \Delta x \cdot m_1 + \Delta y \cdot m_2 + \Delta z \cdot m_3$, $b_1 = (b/a)^2$, $b_2 = (2b/a) \cdot (\Delta x \cdot$

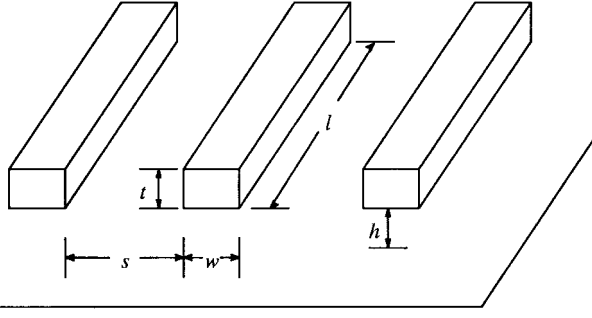


Fig. 3. A configuration of three parallel conductors above a ground plan e , where $l = 20 \mu\text{m}$, $w = 5 \mu\text{m}$, $t = 1 \mu\text{m}$, $h = 2 \mu\text{m}$, $s = 10 \mu\text{m}$, and $\epsilon_1 = \epsilon_2 = 3.9\epsilon_0$.

$\nu_1 + \Delta y \cdot \nu_2 + \Delta z \cdot \nu_3$, $b_3 = a_3$, $b_4 = (b/a) \cdot (\nu_1 \cdot m_1 + \nu_2 \cdot m_2 + \nu_3 \cdot m_3)$, $b_5 = a_5$, $\Delta x = x' - x$, $\Delta y = y' - y$, $\Delta z = z' - z$, $\hat{\mu} = (\mu_1, \mu_2, \mu_3) = (\vec{r}_A - \vec{r}_{i1}) / |\vec{r}_A - \vec{r}_{i1}|$, $\hat{\nu} = (\nu_1, \nu_2, \nu_3) = (\vec{r}_B - \vec{r}_{i1}) / |\vec{r}_B - \vec{r}_{i1}|$, and $\hat{m} = (m_1, m_2, m_3) = (\vec{r}_B - \vec{r}_A) / |\vec{r}_B - \vec{r}_A|$. Therefore, regular integration is reduced to 1-D integral, which is evaluated by Gaussian quadrature method. As the denominator of (13), $\sqrt{a_1\mu^2 + a_2\mu + a_3 + a_4\mu + a_5}$, approaches to zero, the integral will diverge. From (13), the integrand is reduced to (14) by using local coordinate with its original point set to the field point. The integrand can be evaluated by

$$\frac{1}{2} \left(1 - \frac{\mu}{a}\right) \ln \left| \frac{a_1\mu^2 + a_2\mu + a_3}{b_1\mu^2 + b_2\mu + b_3} \right|. \quad (14)$$

The source point $q(x', y', z')$ and the field point $p(x, y, z)$ are space variables, which are described in the rectangular coordinate. It's worth to denote that the dependence of field point in (14) is implicitly related to a_2, a_3, b_2 , and b_3 parameters, which are functions of space variables for source points and field points. \vec{r}_A, \vec{r}_B , and \vec{r}_{i1} are the vectors of the points A, B, and the i th node in the local coordinate. So, $\hat{\mu}$ and $\hat{\nu}$ are the unit vectors from the i th node to the other two neighboring nodes at the τ th element of the arbitrary triangle, as shown in Fig. 2. Since the vectors of \vec{r}_A and \vec{r}_B are specified, \hat{m} can be defined as the unit vector of $\vec{r}_B - \vec{r}_A$.

According to the layout data, an automatic mesh generation takes place, in which node numbers and their coordinates are linked to the pre-processor of finite element tools. Hence, it has been pointed out [21] that the calculated capacitance values are sensitive with respect to selection of nodes. To improve accuracy and efficiency, we propose a sinusoidal weighting scheme within each other of vertex points, $\vec{r}_{i,\text{vertex}1}$ and $\vec{r}_{i,\text{vertex}2}$, in which one takes

$$\vec{r}_{i,k} = \left(\frac{\vec{r}_{i,\text{vertex}2} + \vec{r}_{i,\text{vertex}1}}{2} \right) - \left(\frac{\vec{r}_{i,\text{vertex}2} - \vec{r}_{i,\text{vertex}1}}{2} \right) \cdot \left(\cos \frac{(k-1)\pi}{K} \right)^n \quad (15)$$

where $k = 1, 2, \dots, K$. $\vec{r}_{i,k}$ is the position for k th node of the i th conductor and n is the weighting factor.

TABLE I
COMPARISONS OF COMPUTED CAPACITANCES FOR PARALLEL CONDUCTORS SHOWN IN FIG. 3 USING DIFFERENT METHODS

| Capacitances (in fF) | Ruehli and Brennan [12] | ICPC [8] | SPIDER [9] | BFEM |
|----------------------|-------------------------|----------|------------|----------|
| $C_{11} = C_{33}$ | 4.3 | 4.382 | 4.262 | 4.3573 |
| $C_{12} = C_{23}$ | 0.11 | 0.1098 | 0.1153 | 0.11647 |
| C_{13} | 0.014 | 0.01421 | 0.01436 | 0.014527 |
| C_{22} | 4.1 | 4.290 | 4.165 | 4.2594 |

TABLE II
THE ACCURACY AND CPU TIME VERSUS THE TOTAL MESH NUMBER AND THE EFFECTIVENESS OF SINUSOIDAL WEIGHTING SCHEME FOR FIG. 3

| Number of nodes | n | $C_{11} = C_{33}$ (in fF) | C_{22} (in fF) | $C_{12} = C_{23}$ ($\times 10^{-1}$ fF) | $C_{13} = C_{31}$ ($\times 10^{-2}$ fF) | C_{11} Relative error (%) | CPU time (in sec) |
|-----------------|---|---------------------------|------------------|--|--|-----------------------------|-------------------|
| 54 | | 5.518604 | 5.385476 | 1.612255 | 2.211568 | 24.41 | 9.5 |
| 78 | | 4.738711 | 4.629233 | 1.310679 | 1.687937 | 24.08 | 16.8 |
| 102 | | 4.564680 | 4.460079 | 1.248841 | 1.581599 | 2.91 | 29.5 |
| 270 | | 4.435242 | 4.333217 | 1.214380 | 1.502036 | 1.79 | 230.3 |
| 420 | | 4.357259 | 4.259421 | 1.164679 | 1.452712 | 0.0 | 606.1 |
| †270 | 1 | 4.351573 | 4.252734 | 1.175769 | 1.455277 | 0.13 | 230.6 |
| †270 | 3 | 4.366922 | 4.267646 | 1.181255 | 1.463538 | 0.22 | 234.6 |
| †270 | 5 | 4.383764 | 4.284215 | 1.185010 | 1.472805 | 0.60 | 234.9 |
| †270 | 7 | 4.413000 | 4.312635 | 1.195251 | 1.489463 | 1.28 | 229.9 |
| †270 | 9 | 4.446863 | 4.345402 | 1.208810 | 1.509339 | 2.05 | 230.4 |

† denotes sinusoidal weighting and others indicate equal-space (all case with $k = 10$).

III. RESULTS AND COMPARISONS

In our paper, the accuracy of the proposed method has been checked against existing data of three parallel conductors oriented over an infinite ground plane shown in Fig. 3. Comparisons with these data are made in Table I, where C_{ii} is the ground capacitance and C_{ij} is the coupling capacitance. One can see from front six rows of Table II that the relative error of C_{11} will converge to less than 3% for the number of nodes larger than 102 and the CPU time will be less than 30 s. To investigate the effectiveness of sinusoidal weighting scheme, we calculate the capacitance coefficients for Fig. 3 under different grid-partition conditions, as shown in Table II. The fifth and sixth rows are calculated under equal-space meshing as references for other sinusoidal weighting conditions. From Table II, it can be found that the relative error will grow as n value increases. It is worth to note that under sinusoidal weighting for $n = 1$ the relative error is only about 0.13% but the CPU time is much reduced to about one third of the value under equal-space meshing in the sixth row.

In order to illustrate the flexibility of the proposed technique to more general cases, we consider a combination of parallel conductors, corner, and crossing lines, as shown in the inserts of Figs. 4 and 5. For practical cases, the corner angle of the lower conductor can be arbitrary and the width of the lower conductor at two adjacent parts can be different. The rotation part of the lower conductor is labeled by the dashed line and the fixed part by the solid line. The corner angle is defined as the inner angle between the fixed part and the rotation part of the lower conductor. At first, we calculate

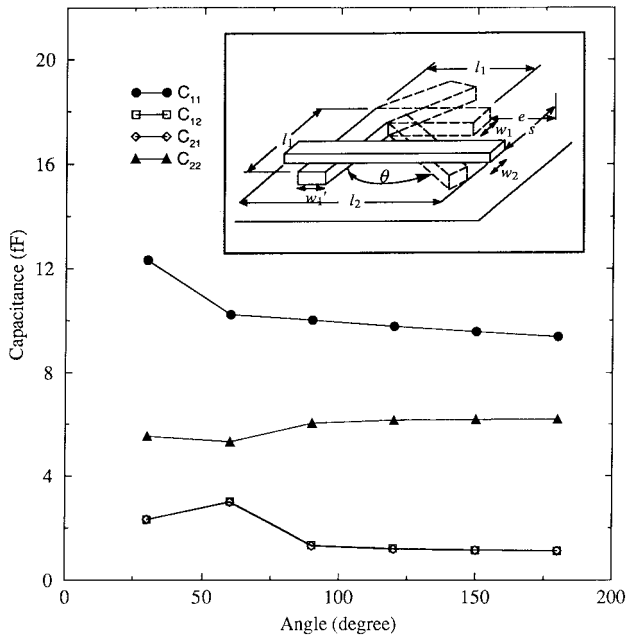


Fig. 4. The computed capacitance versus the corner angle of lower conductor with $w_1' = 3 \mu\text{m}$, and the insert shows combinations of corner and crossing lines: $l_1 = 20 \mu\text{m}$, $w_1 = 3 \mu\text{m}$, $w_1' = 3 \mu\text{m}$, $t_1 = 0.5 \mu\text{m}$, $h_1 = 0.6 \mu\text{m}$, $e = 10 \mu\text{m}$, $l_2 = 20 \mu\text{m}$, $w_2 = 3 \mu\text{m}$, $t_2 = 0.8 \mu\text{m}$, $h_2 = 1.6 \mu\text{m}$, $s = 7 \mu\text{m}$, $\epsilon_1 = 3.9\epsilon_0$, $\epsilon_2 = \epsilon_0$, and $d = 100 \text{ mu}$.

the capacitance values for different corner angles, as shown in the insert of Fig. 4. From the curve shown in Fig. 4, one can see that C_{ij} grows as the angle becomes sharp, due to the increasing accumulation of charge at the convex of corner. Furthermore, there is a peak value of C_{ij} when the angle is around 60° , due to the larger overlap area of two conductors. Secondly, we analyze the capacitances by changing the width of the front part for the lower conductor and keep the angle at 120° , as shown in the insert of Fig. 5. The data points show monotonous variation which is in agreement with our original conjecture, as shown in Fig. 5. The CPU times for the calculations of Figs. 4 and 5 are 441.4 and 441.4 s, respectively, under the corresponding sinusoidal weighting ($K = 6, n = 1$) mesh numbers of 242 and 242, respectively. The computing time depends not only on the algorithm presented here but also on the method of grid partition.

IV. CONCLUSIONS

For the 3-D multilevel interconnection system, the boundary-finite-element technique has been developed as an efficient method to calculate the parasitic capacitance for arbitrary configuration of conductors. In this paper, the existing BFEM of integral formulation is modified and improved. Using arbitrary triangle elements on the surface of conductors for charge distribution, capacitances for more realistic cases with arbitrary configuration of multilevel conductor system in a stratified medium can be efficiently computed. Moreover, we apply the Galerkin principle over finite elements by choosing an adaptive multilevel Green's function and low-order polynomials as shape function. The

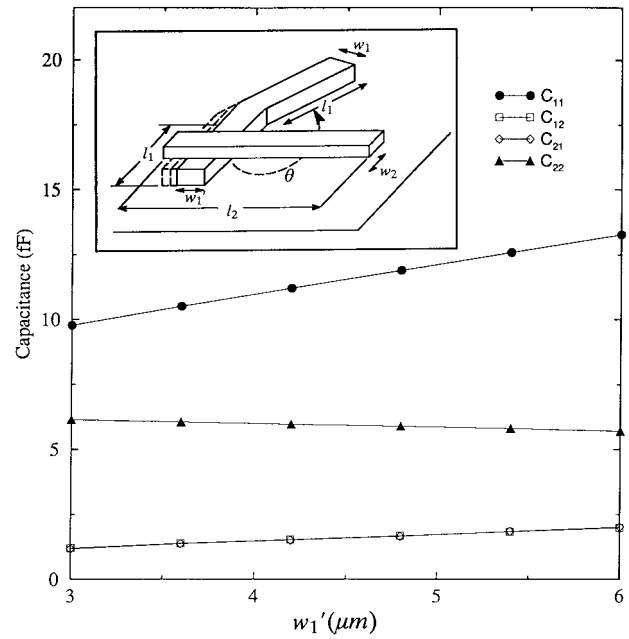


Fig. 5. The computed capacitance versus the width of the front part for the lower conductor with an angle of 120° , and the insert shows combinations of corner and crossing lines: $l_1 = 20 \mu\text{m}$, $w_1 = 3 \mu\text{m}$, $\theta = 120^\circ$, $t_1 = 0.5 \mu\text{m}$, $h_1 = 0.6 \mu\text{m}$, $e = 10 \mu\text{m}$, $l_2 = 20 \mu\text{m}$, $w_2 = 3 \mu\text{m}$, $t_2 = 0.8 \mu\text{m}$, $h_2 = 1.6 \mu\text{m}$, $s = 7 \mu\text{m}$, $\epsilon_1 = 3.9\epsilon_0$, $\epsilon_2 = \epsilon_0$, and $d = 100 \mu\text{m}$.

key points of the proposed BFEM technique are to deduce the analytical form for most of the surface integrals of charge distribution and to eliminate the singular behavior of Class 1 and Class 2 integrals by choosing proper coordinate.

A 3-D capacitance modeling for an arbitrary structure has been developed and confirmed to be efficient and accurate as compared with existing data. Major contributions of the proposed method are adoption of arbitrary triangle elements and elimination of the singular integrals to obtain analytical form. These improvements have made it possible to link with existing CAD tools.

REFERENCES

- [1] J. Rubinstein, P. Penfield, Jr., and M. A. Horowitz, "Signal delay in RC tree networks," *IEEE Trans. Computer-Aided Design*, vol. CAD-2, p. 202, 1983.
- [2] P. Yang, and P. K. Chatterjee, "SPICE modeling for small geometry MOSFET circuits," *IEEE Trans. Computer-Aided Design*, vol. CAD-1, p. 169, 1982.
- [3] C. D. Tayler, G. N. Elkhouri and T. E. Wade, "On the parasitic capacitances of multilevel parallel metallization lines," *IEEE Trans. Electron Devices*, vol. ED-32, p. 2408, 1985.
- [4] W. H. Dierking and J. D. Bastian, "VLSI parasitic capacitance determination by flux tubes," *IEEE Circuits Syst. Mag.*, p. 11, 1982.
- [5] R. H. Uebbing and M. Fukuma, "Process-based three-dimensional capacitance simulation-TRICEPS," *IEEE Trans. Computer-Aided Design*, vol. CAD-5, p. 215, 1986.
- [6] A. Seidel, H. Klose, M. Svoboda, J. Oberndorfer, and W. Rösner, "CAPCAL—A 3-D capacitance solver for support of CAD system," *IEEE Trans. Computer-Aided Design*, vol. 7, p. 549, 1988.
- [7] P. E. Cotrell, E. M. Buturda, and D. R. Thomas, "Multidimensional simulation of VLSI wiring capacitance," in *IEDM Tech. Dig.*, 1982, p. 548.
- [8] Z. Q. Ning, P. M. Dewilde, and F. L. Neerhoff, "Capacitance coefficients for VLSI multilevel metallization lines," *IEEE Trans. Electron Devices*, vol. ED-34, p. 644, 1987.

- [9] Z. Q. Ning and P. M. Dewilde, "SPIDER: Capacitance modeling for VLSI interconnections," *IEEE Trans. Computer-Aided Design*, vol. 7, p. 1221, 1988.
- [10] P. M. Dewilde and Z. Q. Ning, *Models For Large Integrated Circuits*. Norwell, MA: Kluwer, 1990.
- [11] A. E. Ruehli and P. A. Brennan, "Accurate metallization capacitances for integrated circuits and packages," *IEEE J. Solid-State Circuits*, vol. SC-8, p. 289, 1973.
- [12] ———, "Efficient capacitance calculations for three-dimensional multiconductor systems," *IEEE Trans. Microwave Theory Tech.*, vol. MTT-21, p. 76, 1973.
- [13] ———, "Capacitance model for integrated circuit metallization wires," *IEEE J. Solid-State Circuits*, vol. SC-10, p. 530, 1975.
- [14] W. T. Weeks, "Calculation of coefficients of capacitance of multiconductor transmission lines in the presence of a dielectric interface," *IEEE Trans. Microwave Theory Tech.*, vol. MTT-18, p. 35, 1970.
- [15] P. Balaban, "Calculation of the capacitance coefficients of planar conductors on a dielectric surface," *IEEE Trans. Circuit Theory*, vol. CT-20, p. 725, 1973.
- [16] P. Benedek, "Capacitances of a planar multiconductor configuration on a dielectric substrate by a mixed order finite-element method," *IEEE Trans. Circuits Syst.*, vol. CAS-23, p. 279, 1976.
- [17] P. D. Patel, "Calculation of capacitance coefficients for a system of irregular finite conductors on a dielectric sheet," *IEEE Trans. Microwave Theory Tech.*, vol. MTT-19, p. 862, 1971.
- [18] K. Nabors and J. White, "FastCap: A multipole accelerated 3-D capacitance extraction program," *IEEE Trans. Computer-Aided Design*, vol. 10, p. 1447, 1991.
- [19] C. Wei, R. F. Harrington, J. R. Mautz, and T. K. Sarkar, "Multiconductor transmission lines in multilayered dielectric media," *IEEE Trans. Microwave Theory Tech.*, vol. MTT-32, p. 439, 1984.
- [20] J. Venkataraman, S. M. Rao, A. R. Djordjević, T. K. Sarkar, and Y. Naiheng, "Analysis of arbitrarily oriented microstrip transmission lines in arbitrarily shaped dielectric media over a finite ground plane," *IEEE Trans. Microwave Theory Tech.*, vol. MTT-33, p. 952, 1985.
- [21] D. W. Kammler, "Calculation of characteristic admittances and coupling coefficients for strip transmission lines," *IEEE Trans. Microwave Theory Tech.*, vol. MTT-16, p. 925, 1968.
- [22] U. Choudury and A. Sangiovanni-Vincentelli, "Automatic generation of analytical models for interconnect capacitances," *IEEE Trans. Computer-Aided Design*, vol. 14, p. 470, 1995.



Hsin-Ming Hou (S'92) was born in Tainan, Taiwan, R.O.C., on December 29, 1968. He received the B.S. degree from the Physics Department, National Chang Hua Normal University, Changhua, Taiwan, and the M.S. degree from the Institute of Electro-Physics, National Chiao-Tung University, Hsinchu, Taiwan, in 1990 and 1992, respectively. Since 1992, he has been pursuing the Ph.D. degree at the Institute of Electronics, National Chiao-Tung University. His main research interests include computer-aided simulation of electronic circuits and device modeling.



Chin-Shown Sheen (S'92) received the B.S. degree from the Physics Department, National Chang Hua Normal University, Changhua, Taiwan, R.O.C., and the M.S. degree from the Institute of Physics, National Tsing Hua University, Hsinchu, Taiwan, R.O.C., in 1988 and 1990, respectively. He is currently pursuing the Ph.D. degree at the Institute of Electro-Optical Engineering, National Chiao-Tung University. His current research area has been in sensor simulation and device modeling.



Ching-Yuan Wu (S'72–M'75) was born in Taiwan, R.O.C., on March 18, 1946. He received the B.S. degree in electrical engineering from the National Taiwan University, Taipei, in 1968, and the M.S. and Ph.D. degrees from the State University of New York at Stony Brook in 1970 and 1972, respectively.

During the 1972–1973 academic year, he was appointed as a Lecturer in the Department of Electrical Sciences, SUNY-Stony Brook. During the 1973–1975 academic years, he was a Visiting Associate Professor at the National Chiao-Tung University (NCTU), Hsinchu, Taiwan. In 1976, he became Full Professor in the Department of Electronics and the Institute of Electronics at NCTU. While there, he was Director of the Engineering Laboratories and Semiconductor Research Center from 1974 to 1980, the Director of the Institute of Electronics from 1978 to 1984, and the Dean of the College of Engineering from 1984 to 1990. He was a principal investigator of the National Electronics Mass Plan-Semiconductor Devices and Integrated-Circuit Technologies from 1976 to 1979, and had been a Coordinator of the National Microelectronics Researches and High-Level Man-Power Education Committee, National Science Council, R.O.C., from 1982 to 1988. He has been the Research Consultant of the Electronics Research and Service Organization (ERSO), ITRI, a member of the Academic Review Committee in the Ministry of education, and the chairman of the Technical Review Committee on Information and Microelectronics Technologies at the Ministry of Economic Affairs. His research activities have been in semiconductor device physics and modeling, integrated circuit designs, and technologies. His current research areas focus on the development of efficient 2-D and 3-D simulators for deep-submicrometer CMOS devices. He has published over 180 papers in the semiconductor field and has served as a reviewer for international journals such as *IEEE ELECTRON DEVICE LETTERS*, *IEEE TRANSACTIONS ON ELECTRON DEVICES*, and *Solid-State Electronics*.

Dr. Wu is a member of the Honorary Editorial Advisory Board of *Solid-State Electronics*, and is a board member of the Chinese Engineering Society. He received the Academic Research Award in Engineering from the Ministry of Education (MOE) in 1979, and the Outstanding Scholar Award from the Chinese Educational and Cultural Foundation in 1985. He received the Outstanding Research Professor Fellowship from the Ministry of Education and the National Science Council (NSC), R.O.C., from 1982 to 1997. He received the Distinguished Engineering Professor Medal Award from the Chinese Engineering Society in 1992.